Journal of Hazardous Materials 186 (2011) 150–159

Contents lists available at ScienceDirect

Journal of Hazardous Materials

journal homepage: www.elsevier.com/locate/jhazmat

# Removal of fluoride from aqueous solution by polypyrrole/$Fe_3O_4$ magnetic nanocomposite

Madhumita Bhaumik[a], Taile Yvonne Leswifi[a], Arjun Maity[b], V.V. Srinivasu[c], Maurice S. Onyango[a,*]

[a] Department of Chemical and Metallurgical Engineering, Tshwane University of Technology, Pretoria West, Private Bag X680, Pretoria, Gauteng 0001, South Africa
[b] Polymers and Composites, Council for Scientific and Industrial Research (CSIR), Pretoria, South Africa
[c] Mechatronics and Micromanufacturing, Council for Scientific and Industrial Research (CSIR), Pretoria, South Africa

ARTICLE INFO

*Article history:*
Received 15 July 2010
Received in revised form 12 October 2010
Accepted 25 October 2010
Available online 2 November 2010

*Keywords:*
Polypyrrole
Magnetic nanocomposite
Adsorption
Fluoride
Kinetics
Equilibrium

ABSTRACT

Polypyrrole (PPy)/$Fe_3O_4$ magnetic nanocomposite as a novel adsorbent was prepared via *in-situ* polymerization of pyrrole (Py) monomer using $FeCl_3$ oxidant in aqueous medium in which $Fe_3O_4$ nanoparticles were suspended. The adsorbent was characterized by Attenuated Total Reflectance Fourier transform infrared spectroscope (ATR-FTIR), Brunauer–Emmet–Teller (BET) method, field emission scanning electron microscope (FE-SEM), high resolution transmission electron microscope (HR-TEM), X-ray photoelectron spectroscope (XPS) and X-ray diffraction (XRD). Magnetic property of the adsorbent was measured by electron spin resonance (ESR). Subsequently, the ability of the adsorbent to remove fluoride ions from aqueous solution was demonstrated in a batch sorption mode. Results reveal that the adsorption is rapid and that the adsorbent has high affinity for fluoride, which depends on temperature, solution pH and adsorbent dose. From equilibrium modelling, the equilibrium data is well described by Freundlich and Langmuir–Freundlich isotherms while the adsorption kinetics is described by the pseudo-second-order model. Thermodynamic parameters confirm the spontaneity and endothermic nature of the fluoride adsorption. Meanwhile, the fluoride adsorption proceeds by an ion exchange mechanism.



## 1. Introduction

Fluoride has been shown to cause significant effects in human through drinking water. At low concentrations, it has beneficial effects on teeth and bones. However, an excessive exposure to fluoride in drinking water can give rise to a number of adverse effects. These range from mild dental fluorosis to crippling skeletal fluorosis as the level and period of exposure increases. The World Health Organization (WHO) has set the maximum allowable concentration of fluoride in drinking water between 0.5 and 1.5 mg/L [1]. Hence, an excess amount of fluoride in drinking water must be removed using appropriate technologies.

Several technologies have been developed for defluoridation of water, such as adsorption [2–5], precipitation with calcium and aluminium salts [6], ion exchange [7] and membrane processes such as reverse osmosis, nanofiltration, electrodialysis and Donnan dialysis [8–11]. Among these techniques, adsorption is the most widely used method because it is simple, economical and efficient for producing high quality water [12]. The starting point in an adsorption process is to select a media with high capacity and fast kinetics for contaminant removal from water. As such, several adsorbents such as activated alumina [13], activated carbon [14], hydroxyapatite [15], calcite [16], rare earth oxides [17], polyaniline [18] and polypyrrole [19] have been tested in water deflouridation. Most of these media show low capacity and moreover the time- (diffusional time) scale for transferring an adsorbing species in the internal matrix of the adsorbent is relatively large. The latter is due to inherently large diffusion lengths of the conventionally used adsorbents. To overcome this limitation, extensive research has been focused on advance techniques in material design. This new development is responsible for the creation of nano-sized adsorbents.

Advances in nanoscale science and engineering suggest that many of the issues involving water quality could be resolved or greatly improve using nanomaterials [20]. Nanoparticles are one of the important building blocks in the fabrication of nanomaterials. The basic properties, extremely small size and high surface area to volume ratio of nanoparticles provide better kinetics for the adsorption of target contaminants from aqueous solutions. However, the separation of nano-sized particles from solution presents difficulties to a certain extent.

Magnetic separation has been shown to be a very promising method for solid–liquid phase separation technique due to the great advantages, such as effective control [21], high speed, accuracy and simplicity as compared to the conventional separation

* Corresponding author. Tel.: +27 123823533; fax: +27 123823533.
*E-mail addresses:* amaity@csir.co.za (A. Maity), OnyangoMS@tut.ac.za, onyi72uk@yahoo.co.uk (M.S. Onyango).

0304-3894/$ – see front matter © 2010 Elsevier B.V. All rights reserved.
doi:10.1016/j.jhazmat.2010.10.098

method [22]. Hence, recent studies are exploring its application in both drinking and wastewater treatment [23].

In order to remove target pollutants from an aqueous solution, magnetic nanoparticles properties can be tailored by using functionalised polymers to impart surface reactivity. A polymer that has recently attracted research is polypyrrole (PPy). PPy is a conducting polymer with unique properties of high electrical conductivity, relatively good environmental stability, nontoxicity, relatively low cost and ease of preparation, which are favourable for various types of applications in batteries, sensors, supercapacitor, microwave shielding, hybrid materials and as adsorbents [24,25]. It was found that PPy exchange both anions and cations depending upon the polymerization conditions, the type and size of the counterions as well as on the ions present in the electrolyte solution. During polymerization reactions, PPy carries charges via some of the positively charged nitrogen atoms in the polymer matrix. To maintain charge neutrality, some of the counterions are incorporated into the growing polymer chains [26]. The existence of positively charged nitrogen atoms in PPy provides a good prospect for its applications in adsorption or filtration separation [27,28]. PPy has a tendency to aggregate into irregular morphology by the strong $\Pi^*$ interaction between the Py main chain, which is commonly observed in the chemical polymerization technique [29]. To overcome the aggregation of PPy as well as to increase the surface area, nanocomposites are considered as one of the most effective materials because ions can be bonded to the organic polymer/inorganic hybrid nanomaterials [27].

In this work, PPy/$Fe_3O_4$ nanocomposites with magnetic behaviour were synthesized for the removal of fluoride ions from aqueous solution. The magnetic property makes the material easy to retrieve from solution using external magnetic field. The surface area, size, structure and surface properties of the PPy/$Fe_3O_4$ nanocomposite were characterized by BET method, transmission electron microscopy (TEM), scanning electron microscopy (SEM), X-ray diffraction (XRD), and Fourier transform infrared (FTIR) spectroscopy. Magnetic property was characterized by Electron spin resonance (ESR) and adsorption behaviour of fluoride from aqueous solution was examined.

## 2. Experimental procedure

### 2.1. Materials

Pyrrole (Py) was purchased from Sigma–Aldrich, USA and was distilled under reduced pressure prior to use. Ferric Chloride ($FeCl_3$) as oxidant and sodium fluoride (NaF) were also purchased from Sigma–Aldrich, USA. Stock solutions of fluoride were prepared by dissolving NaF in de-ionised water. All other solvents used, were of analytical grade and were freshly distilled before use.

### 2.2. Preparation of the PPy/$Fe_3O_4$ nanocomposites

The PPy/$Fe_3O_4$ nanocomposites were synthesized via *in situ* polymerization of Py monomer in the presence of $FeCl_3$ as oxidant at an ambient temperature where suspended $Fe_3O_4$ nanoparticles were encapsulated by the precipitating PPy moieties as shown in Scheme 1. In a typical polymerization technique, 0.1 g of $Fe_3O_4$ was added into 25 mL deionised water in a conical flask and ultrasonicated for 10 min for better dispersion of $Fe_3O_4$ into water. 3 g of $FeCl_3$, oxidant, was added into the de-ionised water containing $Fe_3O_4$ and was shaken for 10 min. To this mixture, 0.5 mL of pyrrole was syringed. Then the reaction mixture was kept under constant shaking for 3 h at ambient temperature. Finally, to stop the reaction, acetone was added into the reaction mixture. The black powder obtained was filtered and washed with distilled water until the filtrate became colourless and finally washed with acetone. Then the composites were dried at 100 °C for 6 h under vacuum, until the total mass became constant. The total weight of the composites was 0.60 g, determined gravimetrically. The % of PPy contained in the nanocomposite was 83.

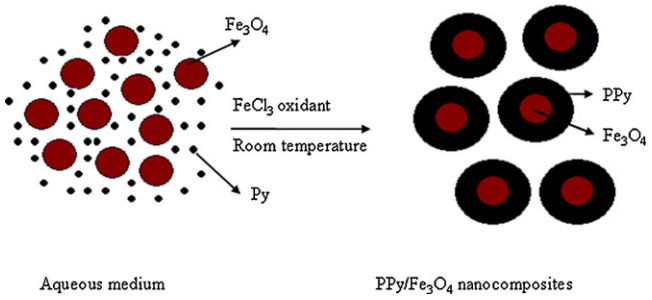


**Scheme 1.** A schematic representation for formation of the PPy/$Fe_3O_4$ nanocomposite.

### 2.3. Characterization of the PPy/$Fe_3O_4$ nanocomposites

Attenuated Total Reflectance (ATR) Fourier transform infrared (FTIR) spectra were recorded on a Perkin-Elmer Spectrum 100 spectrometer, equipped with a FTIR microscopy accessory and a germanium crystal. The BET surface area of the PPy/$Fe_3O_4$ nanocomposite was determined by the low temperature $N_2$ adsorption–desorption technique using Micrometrics. FE-SEM images were obtained on a LEO, Zeiss SEM. The HR-TEM images were obtained on a JEOL JEM-2100 microscopy with a LAB6 filament all operated at 200 kV. Elemental mapping of the nanocomposite was performed using an X-ray photoelectron spectroscopy (XPS) on a Kratos Axis Ultra device, with an Al monochromatic X-ray source (1486.6 eV). X-ray diffraction patterns were measured on a PANalytical X'Pert PRO-diffractometer using Cu Kα radiation (wavelength, λ = 1.5406 Å) with variable slits at 45 kV/40 mA. ESR measurements were carried out using JEOL-ESR spectrometer.

### 2.4. Batch experimental systems

#### 2.4.1. Sorption kinetics

Before any adsorption experiment was done, a stock solution containing 1000 mg $F^-$/L was prepared by dissolving an appropriate amount of NaF in de-ionised water. Experimental solutions for adsorption and analysis were then prepared freshly by diluting the stock solution. Short-term kinetic experiments were carried out by adding 1 g of adsorbent into 1000 mL of fluoride solution, stirred at 350 rpm and operated at 25 °C. The initial fluoride concentration was varied from 10 to 60 mg/L. At time zero and at selected time interval thereafter (up to 120 min), 5 mL samples were withdrawn using a 10 mL syringe and filtered through 0.2 μm cellulose acetate filter. The amount of fluoride adsorbed was calculated using Eq. (1).

$$q_t = \left(\frac{C_0 - C_t}{m}\right) V \quad (1)$$

where $q_t$ is the time-dependent amount of fluoride adsorbed per unit mass of adsorbent (mg/g); $V$ is the volume of solution, $C_0$ is the initial fluoride concentration in solution (mg/L), $C_t$ is the bulk-phase fluoride concentration at any time (mg/L) and $m$ is the adsorbent mass (g).

#### 2.4.2. Sorption equilibrium

Data for sorption isotherm were generated by contacting a fixed mass (0.1 g/50 mL) of the PPy/$Fe_3O_4$ nanocomposites with fluoride-containing aqueous solutions. Samples of 50 mL of the fluoride ion solutions at concentrations ranging from 5 to 100 mg/L were

measured into 100 mL plastic bottles. The bottles were placed in a thermostatic shaker and shaken for one day. The shaking speed was set at 180 revolutions per minute (rpm). Thermodynamic parameters of the adsorption were established by conducting the experiments at 25 °C, 35 °C and 45 °C in a temperature controlled thermostatic shaker. At the end of each experiment, samples were withdrawn from the test bottles, filtered and residual fluoride concentrations were measured (using TISAB) by a fluoride-ion selective electrode. The equilibrium sorption capacity was determined using Eq. (2).

$$q_e = \left(\frac{C_0 - C_e}{m}\right) V \quad (2)$$

where $q_e$ is the equilibrium amount of fluoride adsorbed per unit mass of adsorbent (mg/g) and $C_e$ is the final fluoride concentration (mg/L).

#### 2.4.3. Effect of adsorbent dose

The performance of the PPy/$Fe_3O_4$ nanocomposites in fluoride removal from aqueous solution under different adsorbent doses was tested by varying the amount of the adsorbent from 0.025 to 0.20 g. A given amount of the adsorbent was added to 50 mL of 10 mg/L fluoride solution contained in plastic bottles. The bottles were placed in a thermostatic shaker and were agitated at 180 rpm for 1 day. At the end of the experiment, samples were withdrawn from the test bottles and filtered and thereafter the residual fluoride ion concentration was determined.

#### 2.4.4. Effect of pH

Experiments were carried out by varying initial solution pH values within the range 2–10, using either 0.1 M NaOH or 0.1 M HCl solution. The ionic strength was adjusted using NaCl solution. The experimental procedure and fluoride analysis were similar to those used to generate isotherm data. Accordingly, adsorption was done by adding 0.1 g of the PPy/$Fe_3O_4$ nanocomposites to 50 mL of 10 mg/L fluoride solution contained in plastic bottles. The bottles were placed in a thermostatic shaker and were agitated at 180 rpm for 1 day. At the end of the experiment, fluoride analysis was done.

#### 2.4.5. Effect of co-existing anions

The effect of co-existing anions such as chloride ($Cl^-$), nitrate ($NO_3^-$), sulphate ($SO_4^{2-}$) and phosphate ($PO_4^{3-}$) on fluoride adsorption by the nanocomposites was also investigated. To obtain the equilibrium data for fluoride adsorption in $F^-/Cl^-$, $F^-/NO_3^-$, $F^-/SO_4^{2-}$ and $F^-/PO_4^{3-}$ binary component systems, 0.1 g of the PPy/$Fe_3O_4$ nanocomposites was contacted with 10 mg/L of fluoride solutions for 24 h. The concentrations of co-existing anions were varied from 0 to 80 mg/L. Adsorption experiments were carried out as described in Section 2.4.2.

#### 2.4.6. Desorption study

Desorption studies were performed by using the fluoride adsorbed nanocomposites. Initially, adsorption study was conducted using 2 g/L of the PPy/$Fe_3O_4$ nanocomposites and 10 mg/L of fluoride solution at pH 6.5. Then, desorption experiments were carried out by shaking the fluoride loaded adsorbent with 100 mL of water at different pH values (2–12) for 4 h. The used adsorbent was regenerated by treating with 50 mL of 2 M HCl for 4 h. After regeneration, the ability of the adsorbent to remove fluoride from aqueous solution was again tested using similar procedure as described in Section 2.4.2.

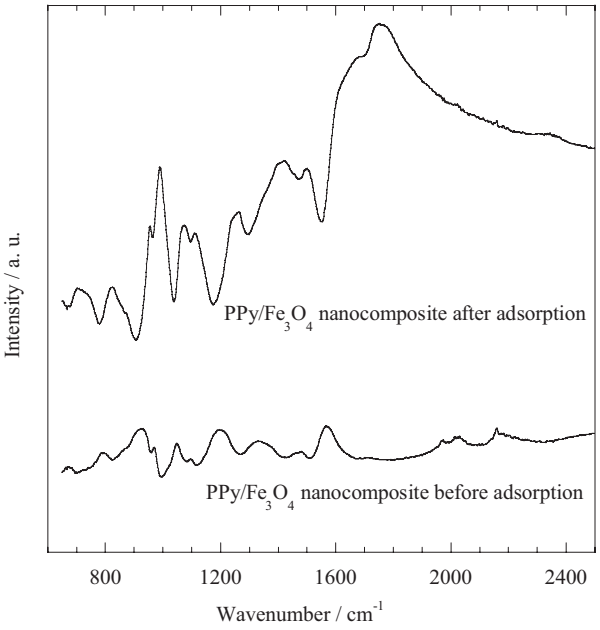


**Fig. 1.** ATR-FTIR spectra of the PPy/$Fe_3O_4$ nanocomposites before and after adsorption with fluoride ions.

## 3. Results and discussion

### 3.1. Characterization of the PPy/$Fe_3O_4$ nanocomposite

The ATR-FTIR spectra of the PPy/$Fe_3O_4$ nanocomposites before and after adsorption with fluoride ions are shown in Fig. 1. On the ATR-FTIR spectrum of PPy homopolymers, the peaks at 1513, 1430, 1082 and 957–825 $cm^{-1}$ are considered to arise from pyrrole ring stretching, conjugated C–N stretching, C–H stretching vibration and C–H deformation, respectively [30]. In contrast, the FTIR spectrum of the PPy/$Fe_3O_4$ nanocomposite demonstrated the peaks at 1513, 1423, 1080 and 958–826 $cm^{-1}$ for pyrrole ring stretching, conjugated C–N stretching, C–H stretching vibration and C–H deformation, respectively. These results confirm the presence of PPy polymeric moieties in the nanocomposite. The PPy component in the nanocomposite after adsorption showed peaks at 1550, 1465, 1096 and 964–863 $cm^{-1}$ for pyrrole ring stretching, conjugated C–N stretching, C–H stretching vibration and C–H deformation, respectively [31,32]. It is interesting to note that all peak positions are shifted towards higher value in case of the PPy/$Fe_3O_4$ nanocomposites after adsorption with fluoride ions. It is well known that the skeletal vibration, which involves the delocalized π-electrons, is affected by the doping ions of the polymer [33]. This feature indicates that the more electronegative fluoride ions adsorbs on the surface of the PPy/$Fe_3O_4$ nanocomposites by replacing doped chloride ions.

The BET surface area of the nanocomposite as determined by low temperature $N_2$ adsorption–desorption method was found to be 1206.53 $m^2/g$. The scanning electron micrographs for (a) $Fe_3O_4$, (b) and (c) PPy/$Fe_3O_4$ nanocomposites before and after adsorption with fluoride are represented in Fig. 2. SEM image of $Fe_3O_4$ (Fig. 2a) reveals the formation of spherical particles and of aggregates with average diameter of 10 nm. In contrast, PPy/$Fe_3O_4$ nanocomposite before adsorption with fluoride shows (Fig. 2b) the formation of nearly spherical particles with larger sizes than those of $Fe_3O_4$ nanoparticles. These features indicate that the formation of polymer based nanocomposites originated from the encapsulation of the nanodimensional $Fe_3O_4$ particle suspensoids in the aqueous medium by the precipitating polymeric moieties. However, the sur-

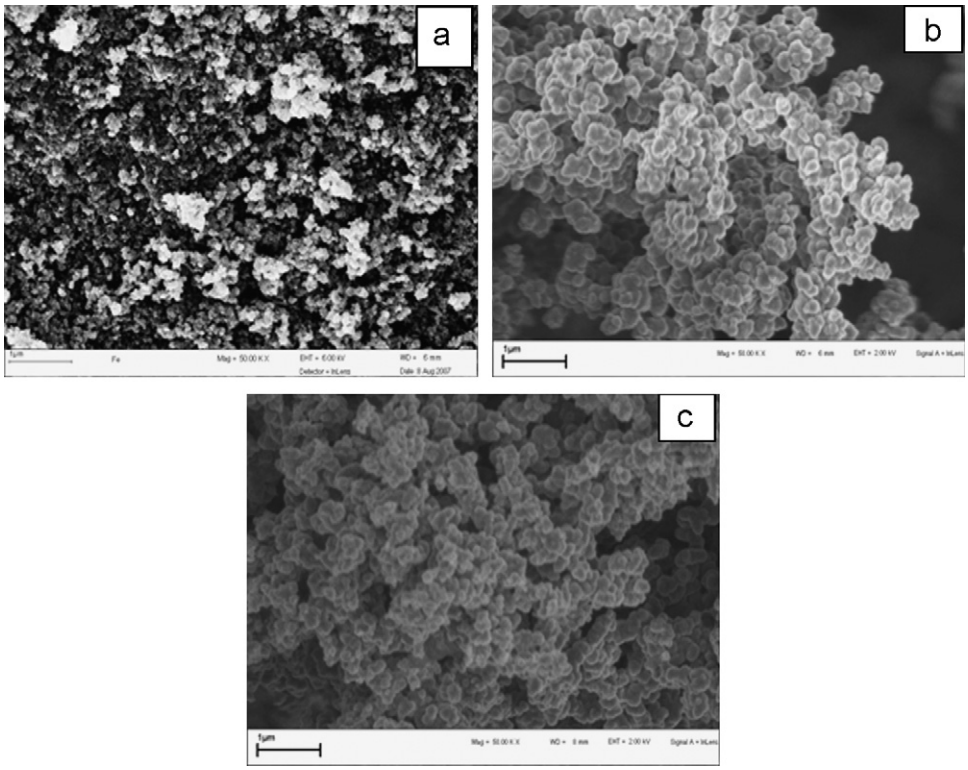


**Fig. 2.** FE-SEM images of (a) $Fe_3O_4$ nanoparticles, (b and c) PPy/$Fe_3O_4$ nanocomposite before and after adsorption with fluoride ions.

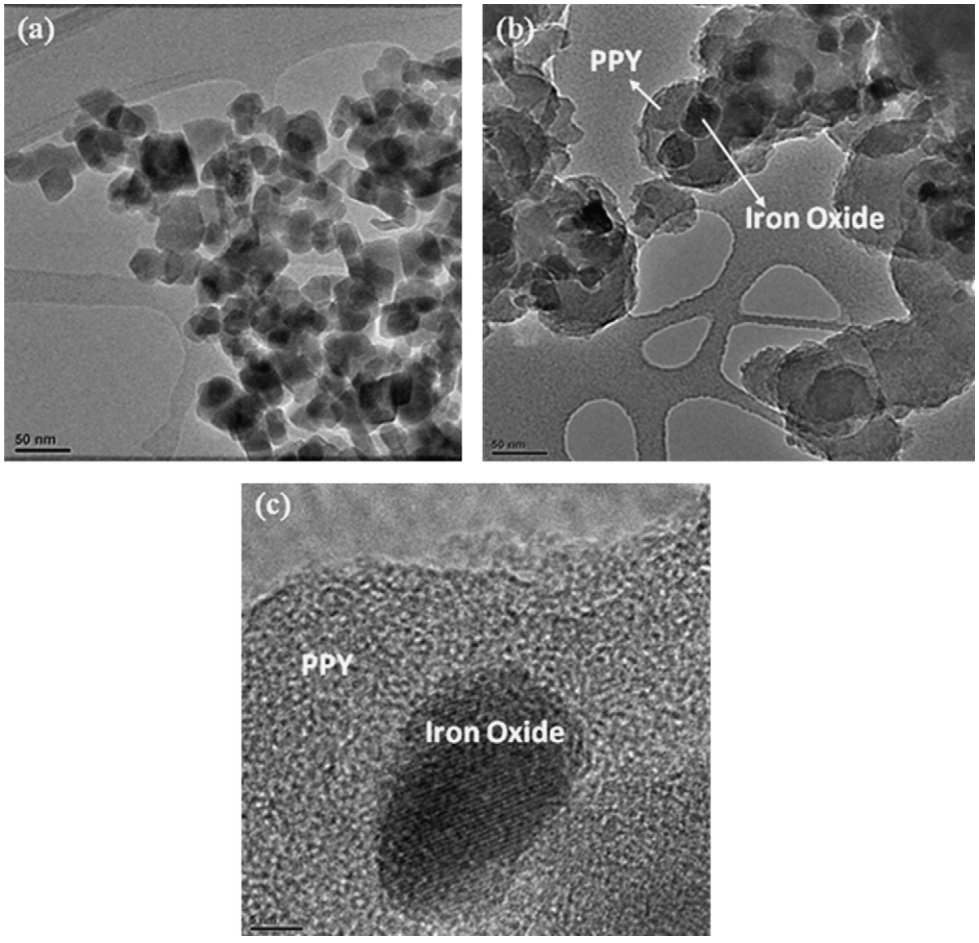


**Fig. 3.** TEM images of (a) $Fe_3O_4$ nanoparticles, (b and c) PPy/$Fe_3O_4$ nanocomposite at two different magnifications.

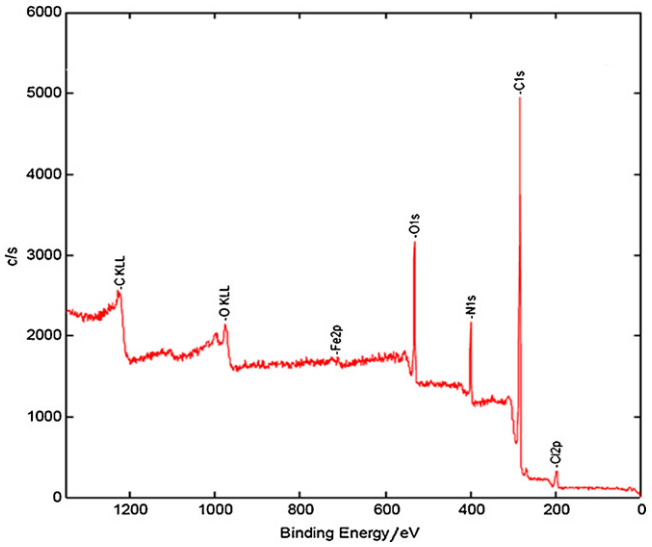


**Fig. 4.** XPS spectrum of PPy/$Fe_3O_4$ nanocomposites.

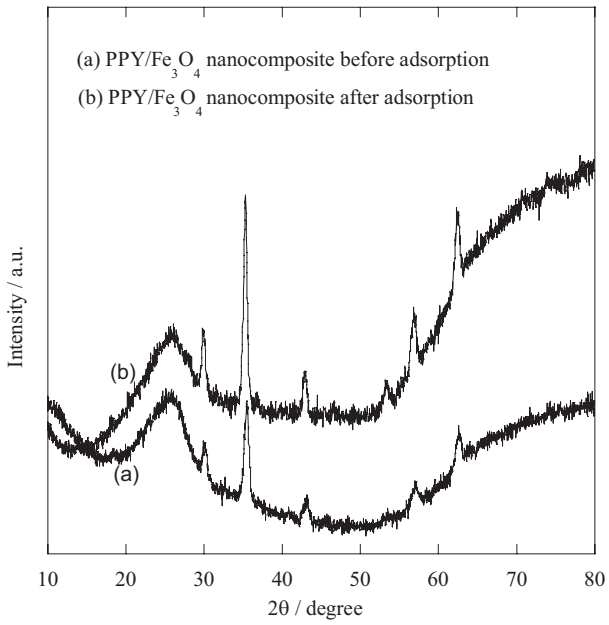


**Fig. 5.** XRD curve of PPy/$Fe_3O_4$ nanocomposite (a) before and (b) after adsorption.

face morphology of the PPy/$Fe_3O_4$ nanocomposites after adsorption (Fig. 2c) with fluoride did not change during adsorption process.

Fig. 3 shows the TEM images of (a) $Fe_3O_4$, and (b) and (c) PPy/$Fe_3O_4$ nanocomposites before adsorption at two different magnifications. As shown in Fig. 3a, $Fe_3O_4$ nanoparticles exist as agglomerates due to high surface area and magneto dipole–dipole interactions between the particles with the average diameter of 10 nm. The TEM images of the nanocomposites indicate that the $Fe_3O_4$ nanoparticles are embedded in the PPy matrix, forming a core–shell structure. The black core is magnetic $Fe_3O_4$ nanoparticles and light coloured shell is PPy in the nanocomposite, due to the different electron penetrability. The TEM results also suggest that nanocomposites formed via encapsulation of $Fe_3O_4$ nanoparticles with precipitating PPy polymeric moieties.

For quantitative estimation of chemical elements of the nanocomposites, XPS studies were undertaken. The survey spectrum of the PPy/$Fe_3O_4$ nanocomposites (Fig. 4) exhibits three major peaks at 532, 400 and 285 eV, corresponding to O 1s, N 1s, and C 1s photoemission. Two minor peaks at 700 and 199 eV corresponding to Fe 2p and Cl 2p photoemissions are also detected. Furthermore, % atomic concentrations of C, O, N, Cl and Fe are 75.8, 13.5, 8.9, 1.7 and 0.2, respectively.

Fig. 5 shows the XRD patterns of the nanocomposite before and after adsorption of fluoride ions. The main peaks at $2\theta = 30.093^\circ$, $35.421^\circ$, $43.050^\circ$, $56.940^\circ$ and $62.510^\circ$ are characteristic peaks of $Fe_3O_4$ [34]. A broad peak at $2\theta = 25^\circ$ is a characteristic peak of PPy [35]. Thus XRD results proved that $Fe_3O_4$ particles existed in the composite. It is evident from Fig. 5 that there is no visual change in the XRD pattern before and after treatment with fluoride. This can be explained by the fact that fluoride ions were removed by the PPy/$Fe_3O_4$ nanocomposites through ion exchange mechanism.

The room temperature ESR spectra for the PPy/$Fe_3O_4$ nanocomposites before (a) and after (b) adsorption of fluoride are shown in Fig. 6. It is clearly seen from the figure that the line shapes are symmetrical and also resonance line is very wide (~100 mT). These kind of large line widths are typical of magnetic particles, due to magnetic inhomogeneity [36–38]. The line shape of the PPy/$Fe_3O_4$ nanocomposites does not fit to a Lorentzian function. In Fig. 7, the best fitting line shape with a mixture of 65% Gaussian and 35% Lorentzian functions is shown. This confirms that the predominant fraction of the PPy/$Fe_3O_4$ nanocomposites is magnetic, as a dominant Gaussian fit is characteristic of ferromagnetic resonance [36]. Fig. 8 shows that the PPy–$Fe_3O_4$ nanocomposites are attracted by the magnetic bar. This further confirms that the nanocomposites are magnetic in nature. The signal intensity of the PPy/$Fe_3O_4$ nanocomposites after fluoride adsorption is 3 times more than that of the signal before adsorption (from Fig. 7). At present, we do not understand the origin of this effect but it shows that ESR is very useful to probe the fluoride (impurity) adsorption from water by the PPy/$Fe_3O_4$ magnetic nanoparticles. Future experiments will be done to quantify and calibrate this procedure for fluoride adsorption analysis.

### 3.2. Sorption kinetics

The effect of time and initial concentration on the uptake of fluoride is shown in Fig. 9. It can be seen that the kinetics of fluoride

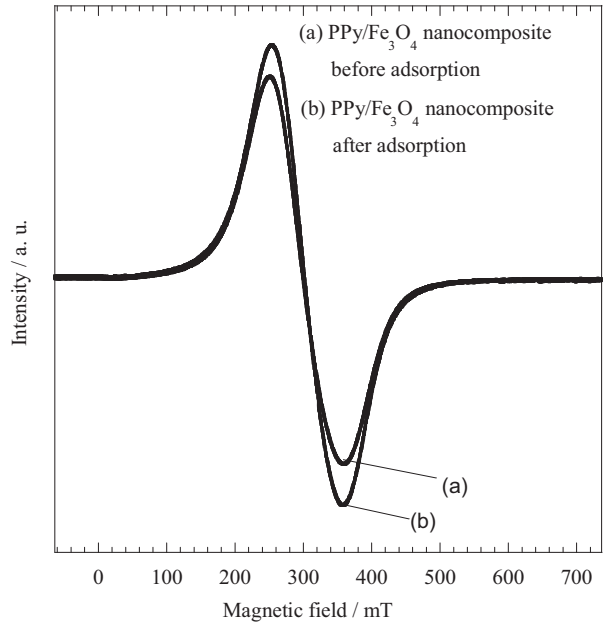


**Fig. 6.** Derivative ESR absorption signals versus magnetic field (H) for (a) PPy/$Fe_3O_4$ nanocomposite before adsorption (gain $2 \times 10^1$) and (b) PPy/$Fe_3O_4$ nanocomposite after adsorption (gain $3 \times 1$).

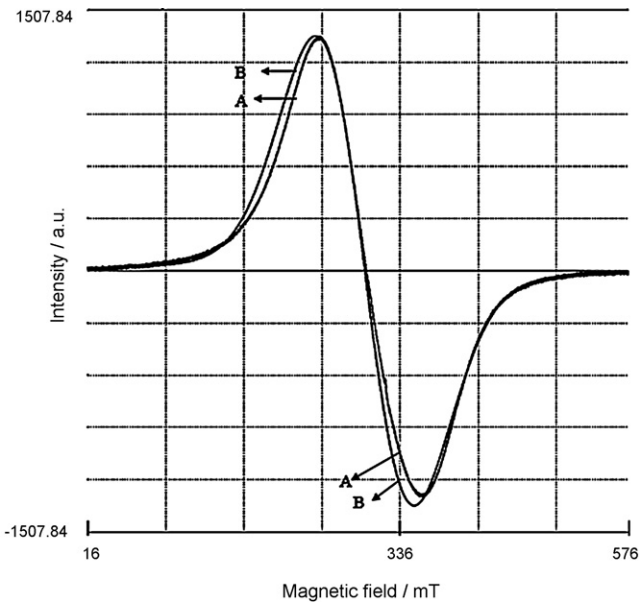


**Fig. 7.** ESR spectra of (A) PPy/$Fe_3O_4$ nanocomposite and (B) 35% Lorentzian–65% Gaussian fitting at 20 °C.

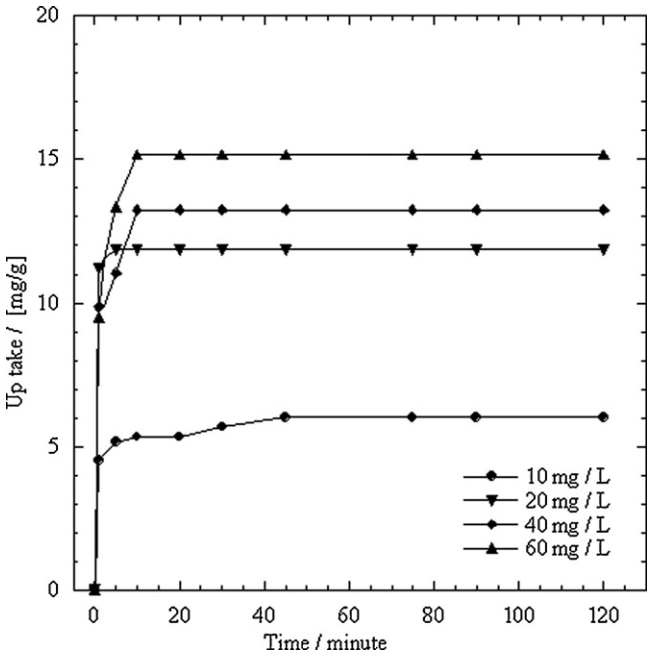


**Fig. 9.** Kinetic data for fluoride adsorption on the PPy/$Fe_3O_4$ nanocomposite at 25 °C.

uptake was very fast initially followed by a slightly slower rate that gradually led to an equilibrium condition in about 20 min for all the concentrations studied. The time to reach equilibrium condition was shorter compared to those of other reported adsorbents such as activated alumina, 6 h [13]; rare earth oxides, 40 min [17]; hydrous ferric oxide, 60 min [39]; nano-hydroxyapatite, 100 min [40]; aligned-carbon nanotubes, 180 min [41]; $Fe_3O_4$@$Al(OH)_3$ magnetic nanoparticles, 60 min [42].

The rapidity in the uptake kinetics can be explained in terms of reduction in diffusion path and increase in exposed surface area. As material tends towards nano-scale size, the distance an adsorbing species travels to reach the active sites is significantly reduced, the external surface area per unit mass is increased and hence the adsorbing species experiences reduced diffusion resistance leading to faster kinetics. Moreover, at nano-scale size most of the adsorption sites in the PPy/$Fe_3O_4$ nanocomposites exist in the exterior surface where they are easily accessible to the adsorbing fluoride. Meanwhile, the fluoride uptake increased with an increase in initial concentration. Apparently, adsorption is a passive process driven

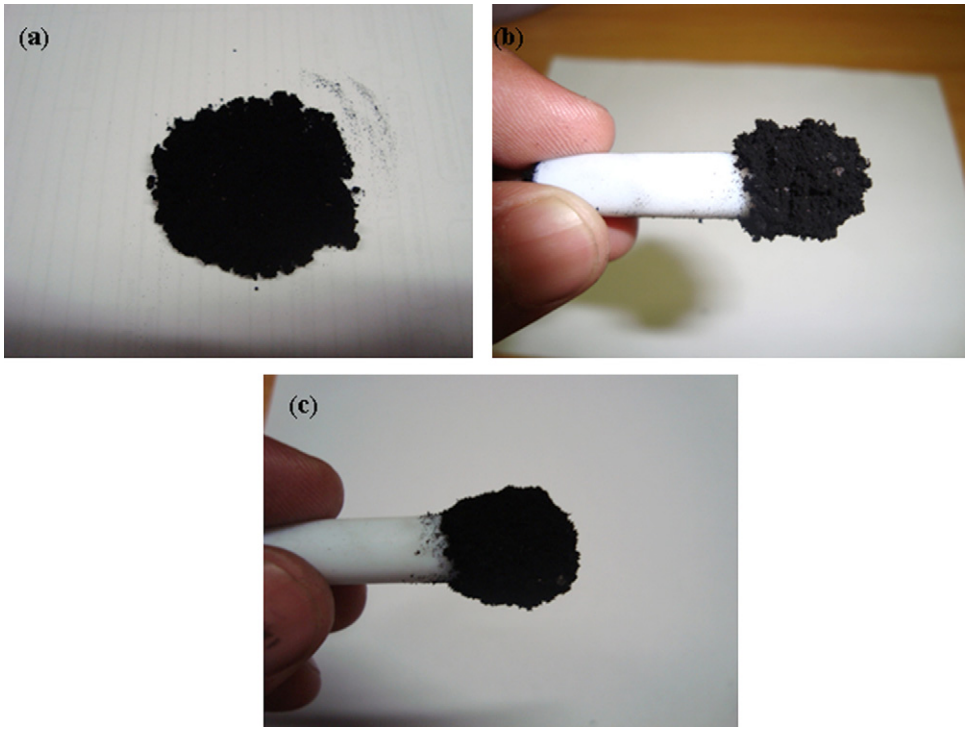


**Fig. 8.** Photographs of (a) PPy/$Fe_3O_4$ nanocomposites, (b and c) PPy/$Fe_3O_4$ nanocomposites attract by magnetic bar before and after adsorption.

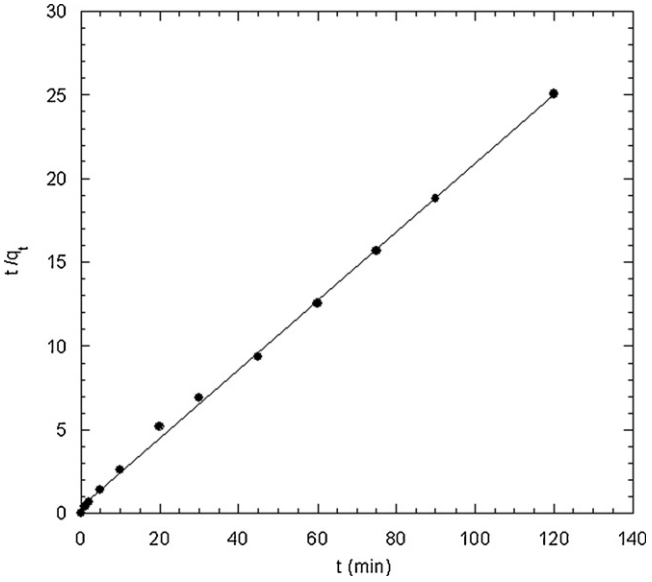


**Fig. 10.** Fit of kinetics data to pseudo-second-order model.

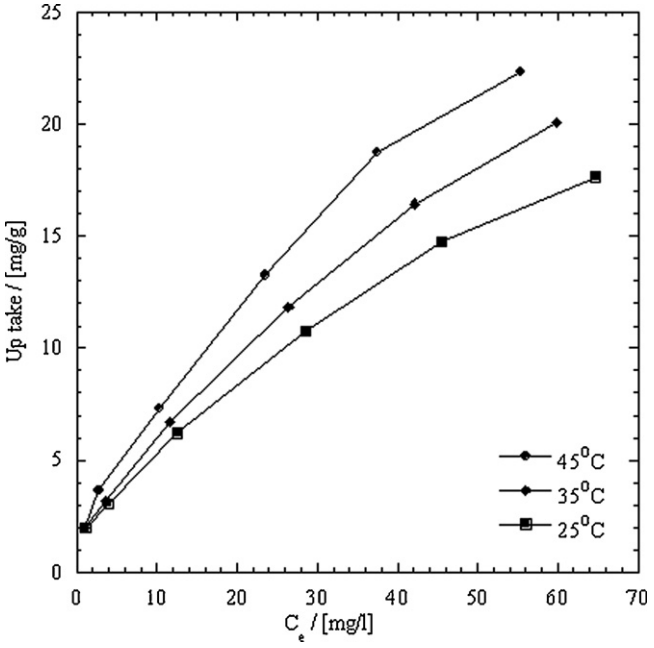


**Fig. 11.** Adsorption isotherms of fluoride onto PPy/$Fe_3O_4$ nanocomposite.

by concentration gradient as a driving force. The higher the initial concentration the higher is the driving force leading to a higher uptake rate.

The kinetics data of fluoride adsorption by the PPy/$Fe_3O_4$ were fitted with the pseudo-second-order kinetic model given in Eq. (3).

$$\frac{t}{q_t} = \frac{1}{k_2 q_e^2} + \frac{1}{q_e} t \tag{3}$$

where $k_2$ is the rate constant of adsorption (g/mg/min), $q_t$ is the amount of fluoride adsorbed at any time (mg/g) and $q_e$ is equilibrium adsorption capacity (mg/g). Fig. 10 shows a typical experimental data fit of the pseudo-second-order model for the initial concentration of 10 mg/L. The data points fit very well to the model with regression coefficients, $R^2 = 0.998$. The constant related to the adsorption rate $k_2$, is 0.11, 0.85, 0.25 and 0.14 g/mg/min for 10, 20, 40 and 60 mg/L, respectively. The predicted $q_e$ values are 4.9, 11.6, 13.2 and 15.9 mg/g for 10, 20, 40 and 60 mg/L, respectively. The predicted equilibrium uptakes are close to the experimental values indicating the applicability of the pseudo second order model.

### 3.3. Sorption isotherms

To evaluate the adsorption capacity of a material and to design and operate an adsorption process efficiently, equilibrium data is a prerequisite. Moreover, information derived from such data is important in comparing different adsorption media. Fig. 11 shows a plot of solid-phase concentration (mg/g) against bulk-phase concentration (mg/L) as a function of temperature. It is observed that the uptake of fluoride increases significantly as temperature is increased. Such observation has been reported for several fluoride sorption systems [43–45] and indicates that the fluoride interaction with PPy/$Fe_3O_4$ nanocomposites is endothermic in nature. The fluoride adsorption capacity of the nanocomposites was found to be within the range of 17.63–22.31 mg/g. Table 1 represents a comparison of adsorption capacity with some other adsorbents reported earlier. It is very difficult to compare directly with other adsorbents because of the different applied experimental condition. However, the fluoride uptake value obtained in this study is reasonable higher than those of other adsorbents.

The equilibrium data were further fitted to isotherms such as the Freundlich, Langmuir, Langmuir–Freundlich, Redlich–Peterson and Dubinin–Radushkevitch. Of these isotherms, only the Freundlich and the Langmuir–Freundlich models described the equilibrium data satisfactorily. The Freundlich isotherm is given by

$$q_e = K_F C_e^{1/n} \tag{4}$$

where $K_F$ and $1/n$ are parameters related to adsorption capacity and surface heterogeneity, respectively. The linear form of Eq. (4) is given by

$$\ln q_e = \ln K_F + \frac{1}{n} \ln C_e \tag{5}$$

Fig. 12 shows the experimental data fit to the linearized form of the Freundlich model. The data points fit very well to the model with regression coefficients, $R^2 \approx 0.99$ for all the temperatures studied. The constant related to the adsorption capacity $K_F$, is 1.66, 1.76 and 1.95 for 25 °C, 35 °C and 45 °C, respectively. The $K_F$ values confirm that adsorption is favoured at high temperature. The heterogeneity coefficient, $1/n$, on the other hand is 0.45, 0.48 and 0.47 for 25 °C, 35 °C and 45 °C, respectively. The $1/n$ values suggest heterogeneous sorption sites. Meanwhile the three-parameter model, Langmuir–Freundlich, given in Eq. (6) was tested in the linear form expressed in Eq. (7)

$$q_e = \frac{K_{LF} C_e^{1/n}}{1 + a_{LF} C_e^{1/n}} \tag{6}$$

**Table 1**
Comparison of fluoride adsorption capacity of various materials.

| Adsorbent | Adsorption capacity (mg/g) | pH | Reference |
|---|---|---|---|
| Activated alumina | 3.86–5 | 6.0 | [13] |
| Activated carbon | 2.5 | 3.5 | [14] |
| Hydrous ferric oxide | 16.5 | 5.0 | [39] |
| Nano-hydroxyapatite | 0.0702–6.161 | 5.0 | [40] |
| Aligned carbon nanotubes | 4.1 | 7.0 | [41] |
| $Al_2O_3$/CNTs | 14.9 | 6.0 | [46] |
| Magnetic-chitosan | 3.0–17 | 7.0 | [47] |
| Polyaniline | 0.77 | – | [18] |
| Polypyrrole | 6.37 | – | [19] |
| PPy/$Fe_3O_4$ | 17.6–22.3 | 6.5 | Present study |

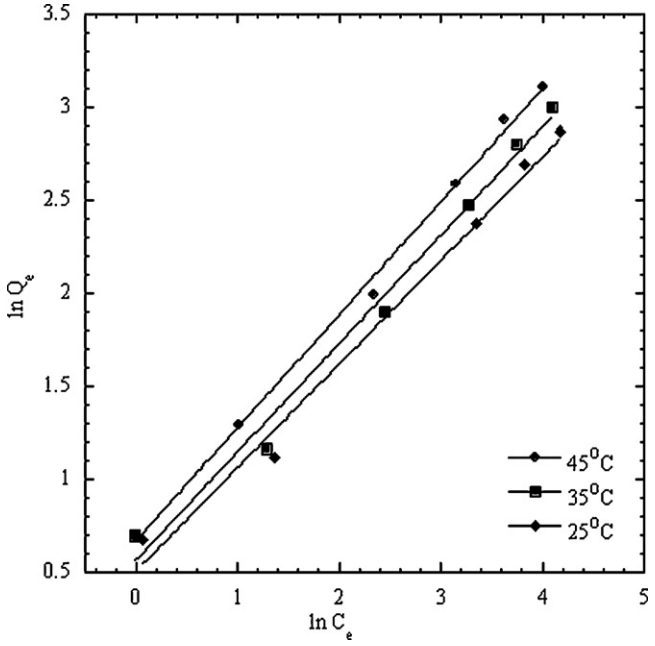


**Fig. 12.** Fit of equilibrium data to Freundlich isotherm model.

$$\ln\left[\frac{1}{q_e} - \frac{a_{LF}}{K_{LF}}\right] = -\ln K_{LF} - \frac{1}{n}\ln C_e \quad (7)$$

where $K_{LF}$ is the Langmuir–Freundlich constant and $a_{LF}$ is the affinity coefficient. The Langmuir–Freundlich plot according to Eq. (7) is shown in Fig. 13. The parameters $K_{LF}$ and $1/n$ were determined from the intercepts (extrapolated to $\ln C_e = 0$) and slopes of the linear curves shown in the figure. At 25 °C, for example, the $K_{LF}$, $1/n$ and $a_{LF}$ values are 1.66, 0.56 and 0.0017, respectively. These parameters show an increase trend with an increase in temperature. Since $a_{LF}$ values are very small, the $K_{LF}$ and $1/n$ are in the same order of magnitude as those computed from the Freundlich isotherm.

The thermodynamic parameters: changes in entropy ($\Delta S^0$) and enthalpy ($\Delta H^0$) for the adsorption of fluoride (at initial concentration of 100 mg/L) over the sorption media were determined by

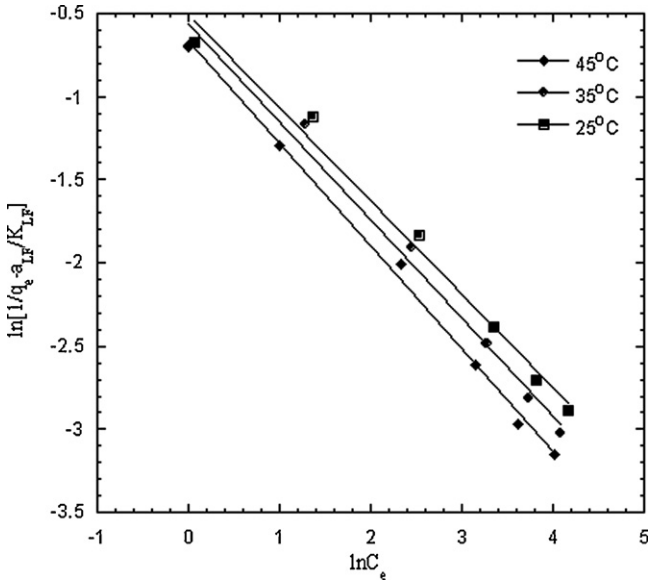


**Fig. 13.** Fit of equilibrium data to Langmuir–Freundlich model.

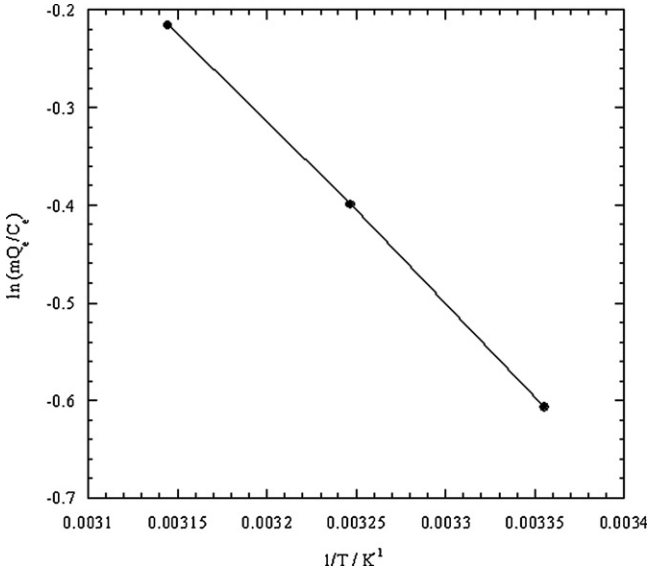


**Fig. 14.** Plot to determine thermodynamic parameters of fluoride adsorption on the PPy/$Fe_3O_4$ nanocomposite.

using the following equation:

$$\ln\left(\frac{mQ_e}{C_e}\right) = \frac{\Delta S^0}{R} + \frac{-\Delta H^0}{RT} \quad (8)$$

where $m$ is the adsorbent dose (g/L), $Q_e$ is the amount of fluoride adsorbed per unit mass of adsorbent (mg/g), $C_e$ is the equilibrium concentration (mg/L) and $T$ is the temperature in K. The ratio $mQ_e/C_e$ is referred to as adsorption affinity. Fig. 14 shows the plot of $\ln(mQ_e/C_e)$ versus $1/T$ according to Eq. (7). Both the change in enthalpy ($\Delta H^0$) and the entropy ($\Delta S^0$) of adsorption are obtained from the plot of $\ln(mQ_e/C_e)$ versus $1/T$ and the values are 15.4 kJ/mol and 46.71 J/mol K, respectively. The positive value of $\Delta H^0$ is consistent with the endothermic nature of the sorption process while the positive value of $\Delta S^0$ suggests an increase in disorder at the solid–liquid interface. From the values of change in enthalpy and entropy, the change in standard Gibbs energy was computed and found to decrease from 1.48 kJ/mol at 25 °C to 0.55 kJ/mol at 45 °C, which infers to a spontaneous process.

### 3.4. Effect of dose

The effect of the PPy/$Fe_3O_4$ nanocomposites dose on fluoride removal from aqueous solution is shown in Fig. 15. It is shown that percentage fluoride removal increases with an increase in PPy/$Fe_3O_4$ dose. Specifically, the extent of fluoride removal changes from 30% at a dose of 0.025 g to 80% at a dose 0.200 g of PPy/$Fe_3O_4$. The increase in the amount of the PPy/$Fe_3O_4$ nanocomposites significantly influenced the extent of fluoride adsorption due to the increase in the number of active sites available for adsorption.

### 3.5. Effect of pH

Fluoride adsorption behaviour of the PPy/$Fe_3O_4$ nanocomposites was explored under different pH conditions to understand further the fluoride removal mechanism and to determine the pH region of maximum performance of the nanomaterial. Results are shown in Fig. 16. It is observed that fluoride uptake increases with an increase in solution pH from 2 to 6. Above pH 6, there is a slight decrease in fluoride uptake. Such a trend has been reported for several sorbent–fluoride sorption systems [48,49]. In the low pH region, the low fluoride uptake is due to reduced availability of free fluoride ions while the slight reduction at high pH may result from

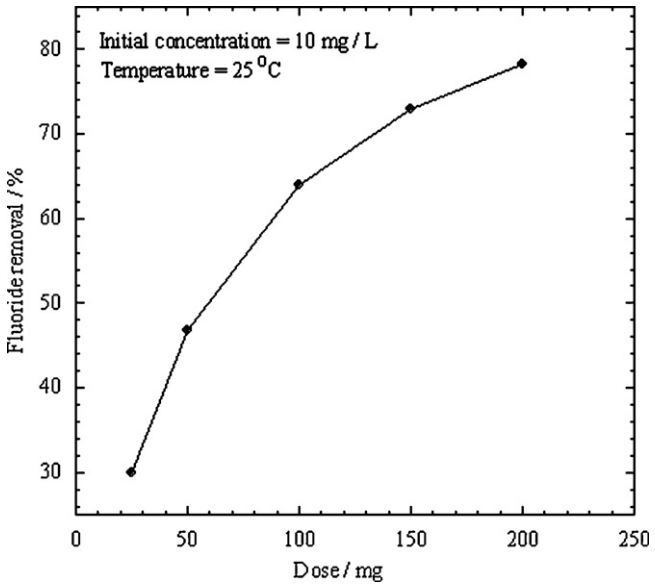


**Fig. 15.** Effect of adsorbent dosage on the removal of fluoride by PPy/$Fe_3O_4$ nanocomposite.

competitive interaction with hydroxyl ions and electrostatic repulsion between some deprotonated active sites and fluoride. Overally, results suggest that the nanocomposite is more effective in the near neutral and alkaline pH range. Drinking water pH normally ranges from 6.5 to 8.5 and hence the nanocomposite is expected to perform optimally in drinking water defluoridation. For wastewater, pH adjustment may be required for optimal performance.

### 3.6. Effect of co-existing anions

Generally drinking water contains several anions like chloride, nitrate, sulphate, and phosphate. The effect of these co-existing anions on fluoride adsorption was also investigated and the results are shown in Fig. 17. It was found that the presence of chloride and

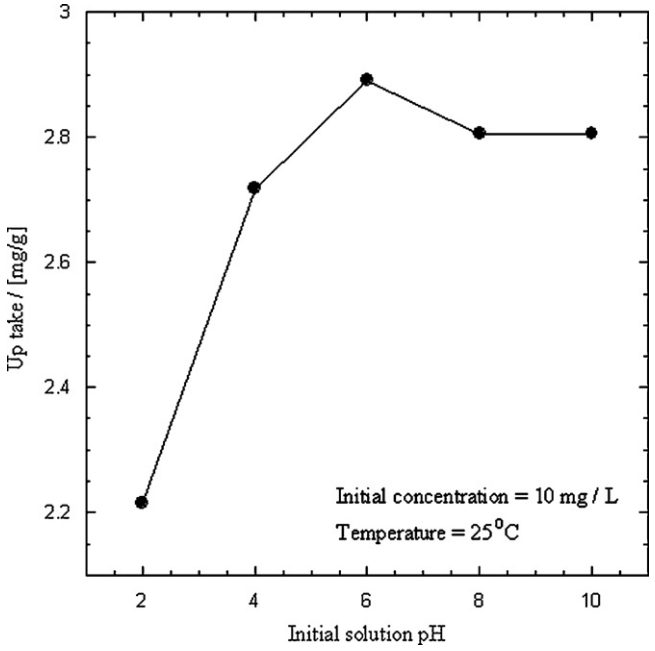


**Fig. 16.** Effect of pH on the removal of fluoride by PPy/$Fe_3O_4$ nanocomposite.

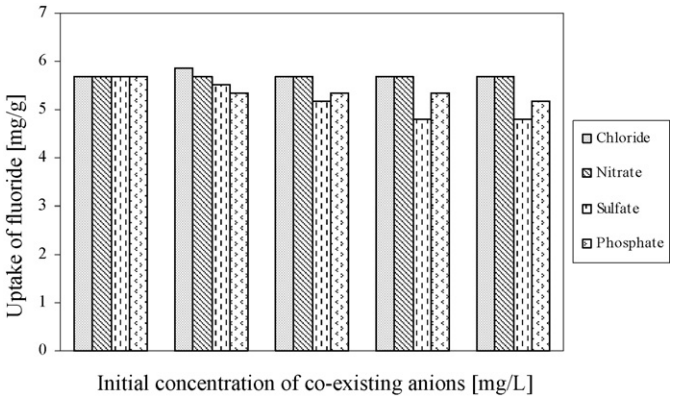


**Fig. 17.** Effect of co-existing anions on the removal of fluoride by PPy/$Fe_3O_4$ nanocomposite.

nitrate ions has negligible effect on fluoride adsorption. The presence of sulphate and phosphate ions slightly reduced the fluoride adsorption due to competitive interaction. This can be explained by the fact that fluoride, sulphate and phosphate ions are all inner-sphere complex-forming species and therefore competed for the same active sites of adsorption [48].

### 3.7. Desorption

To develop a cost effective adsorbent for fluoride removal, it is important that the adsorbed fluoride should be easily desorbed for reusability of the media. Desorption of fluoride from loaded nanocomposite was conducted under different pHs and the results are shown in Fig. 18. In the acidic pH range, small amount of fluoride was eluted from the media while in the alkaline pH range a significant elution was observed. Specifically, 97% of the adsorbed fluoride was released at pH 12. The adsorption capacity of the regenerated adsorbent from a 10 mg/L of fluoride solution was found to be 3.05 mg/g (results not shown). This value is the same as the amount obtained in the first adsorption cycle. As such, the results indicate the recyclability of the material for further use. However, more adsorption tests and characterization are required to determine the exact life cycle of the adsorbent.

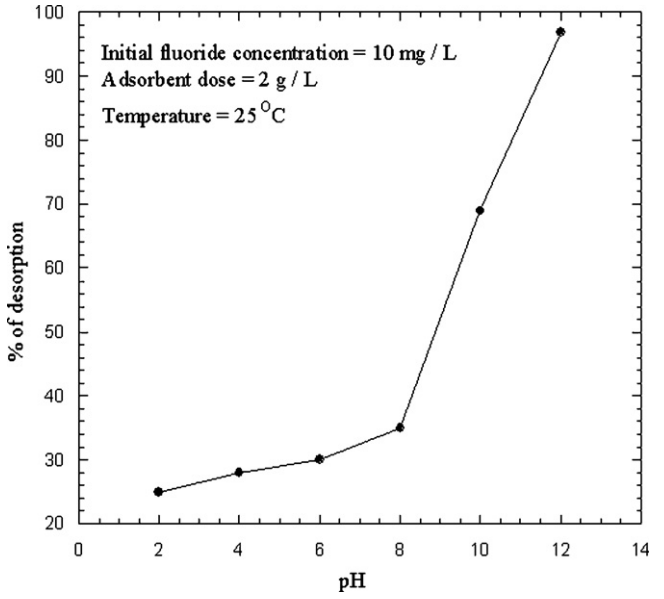


**Fig. 18.** Desorption of fluoride adsorbed PPy/$Fe_3O_4$ nanocomposite under different pH values.

## 4. Conclusions

Magnetic adsorption process provides a cost effective and environmentally benign water treatment process. Consequently, a novel nanocomposite with magnetic property combining both polypyrrole and $Fe_3O_4$ was prepared, characterized and applied in the removal of fluoride as a model contaminant in water. The material was effective in water defluoridation. The fluoride uptake was very rapid and depended on the initial concentration, temperature, adsorbent dose and pH. The adsorption kinetics was described by the pseudo-second-order kinetic model. The adsorption process was endothermic in nature and proceeded by ion exchange mechanism. The equilibrium data fitted well to the Freundlich and Langmuir–Freundlich models. Adsorption of fluoride in the presence of other anions such as chloride, nitrate, sulphate and phosphate was not affected remarkably. Up to 97% of the adsorbed fluoride on the PPy/$Fe_3O_4$ nanocomposites was desorbed at pH 12. The adsorbent retained the original adsorption capacity after one complete adsorption–desorption cycle, confirming the reusability of the nanocomposite for fluoride removal. Further tests are still required to determine the robustness of the material and to possibly upgrade to magnetic adsorption process.

## Acknowledgement

The authors acknowledge the partial financial support offered by National Research Fund (NRF) of South Africa under the Nanoflagship Project Support.

## References

[1] World Health Organization (WHO), Guidelines for Drinking-Water Quality, vol. 1, third ed., WHO, Geneva, 2004.
[2] K.P. Elango, V. Gopal, Equilibrium, kinetic and thermodynamic studies of adsorption of fluoride onto plaster of Paris, J. Hazard. Mater. 141 (2007) 98–105.
[3] M.S. Onyango, Y. Kojima, O. Aoyi, E.C. Bernardo, H. Matsuda, Adsorption equilibrium modeling and solution chemistry dependence of fluoride removal from water by trivalent-cation-exchanged zeolite F-9, J. Colloid Interface Sci. 279 (2004) 341–350.
[4] E.J. Reardon, Y. Wang, Limestone reactor for fluoride removal from wastewaters, Environ. Sci. Technol. 34 (2000) 3247–3253.
[5] S. Saha, Treatment of aqueous effluent for fluoride removal, Water Res. 27 (1993) 1347–1350.
[6] N. Parthasarathy, J. Buffle, W. Haerdi, Combined use of calcium salts and polymeric aluminium hydroxide for defluoridation of waste waters, Water Res. 20 (1986) 443–448.
[7] G. Sing, B. Kumar, P.K. Sen, J. Maunder, Removal of fluoride from spent pot liner leachate using ion exchange, Water Environ. Res. 71 (1999) 36–42.
[8] S.V. Joshi, S.H. Meheta, A.P. Rao, A.V. Rao, Estimation of sodium fluoride using HPLC in reverse osmosis experiments, Water Treat. 7 (1992) 207–210.
[9] R. Simon, Trace element removal from ash dam waters by nanofiltration and diffusion dialysis, Desalination 89 (1993) 325–341.
[10] S.K. Adhikary, U.K. Tipnis, W.P. Harkare, K.P. Govindon, Defluoridation during desalination of brackish water by electrodialysis, Desalination 71 (1989) 301–312.
[11] T. Ruiz, F. Persin, M. Hichour, J. Sandeaux, Modelisation of fluoride removal in Donnan dialysis, J. Membr. Sci. 212 (2003) 113–121.
[12] M.S. Onyango, H. Matsuda, Fluoride removal from water using adsorption technique, in: A. Tressaud (Ed.), Fluoride and Environment, vol. 2, Elsevier B.V., The Netherlands, 2006, pp. 1–48.
[13] C. Venkobacher, L. Iyengar, Defluoridation of water using activated alumina – a report, UNICEF Project No. CE/UNICEF/9132, 1998.
[14] R.L. Ramos, J.O. Turrubiartes, M.A.S. Castillo, Adsorption of fluoride from aqueous solution on aluminium-impregnated carbon, Carbon 37 (1999) 609–617.
[15] S. Gao, J. Cui, Z. Wei, Study on fluoride adsorption of various apatite materials in aqueous solution, J. Fluorine Chem. 130 (2009) 1035–1041.
[16] M. Srimurali, A. Pragathi, J. Karthikeyan, A study on removal of fluorides from drinking water by adsorption onto low-cost materials, Environ. Pollut. 99 (1998) 285–289.
[17] A.M. Raichur, M.J. Basu, Adsorption of fluoride onto mixed rare earth oxides, Sep. Purif. Technol. 24 (2001) 121–127.
[18] M. Karthikeyan, K.K. Satheeshkumar, K.P. Elango, Defluoridation of water via doping of polyanilines, J. Hazard. Mater. 163 (2009) 1026–1032.
[19] M. Karthikeyan, K.K. Satheeshkumar, K.P. Elango, Removal of fluoride ions from aqueous solution by conducting polypyrrole, J. Hazard. Mater. 167 (2009) 300–305.
[20] N. Savage, M.S. Diallo, Nanomaterials and water purification: opportunities and challenges, J. Nanopart. Res. 7 (2005) 331–342.
[21] S.R. Rudge, T.L. Kurt, C.R. Vessely, L.G. Catterall, D.L. Williamson, Preparation, characterization, and performance of magnetic iron–carbon composite microparticles for chemotherapy, Biomaterials 21 (2000) 1411–1420.
[22] Z.G Peng, K. Hidajat, M.S. Uddin, Adsorption of bovine serum albumin on nanosized magnetic particle, J. Colloid Interface Sci. 271 (2004) 277–283.
[23] D.K. Tiwari, J. Behari, P. Sen, Application of nanoparticles in wastewater treatment, World Appl. Sci. J. 3 (2008) 417–423.
[24] T.M. Wu, S.H. Lin, Synthesis, characterization and electrical properties of polypyrrole/multiwalled carbon nanotube composites, J. Polym. Sci. A: Polym. Chem. 44 (2006) 6449–6457.
[25] G. Han, J. Yuan, G. Shi, F. Wei, Electrodeposition of polypyrrole/multiwalled carbon nanotube composite films, Thin Solid Films 474 (2005) 64–69.
[26] X. Zhang, R. Bai, Surface electric properties of polypyrrole in aqueous solutions, Langmuir 19 (2003) 10703–10709.
[27] X. Zhang, R. Bai, Y.W. Tong, Selective adsorption behaviors of proteins on PPy-based adsorbents, Sep. Purif. Technol. 52 (2006) 161–169.
[28] B. Saoudi, N. Jammul, M.L. Abel, M.M. Chehimi, G. Dodin, DNA adsorption onto conducting polypyrrole, Synth. Met. 87 (1997) 97–103.
[29] J. Mansouri, R.P. Burford, Novel membranes from conducting polymers, J. Membr. Sci. 87 (1994) 23–34.
[30] A. Maity, S. Sinha Ray, Highly conductive core–shell nanocomposite of polyN-vinylcarbazole–polypyrrole with multiwall carbon nanotubes, Macromol. Rapid Commun. 29 (2008) 1582–1587.
[31] J. Jang, Y. Nam, H. Yoon, Fabrication of polypyrrole–poly(N-vinylcarbazole) core–shell nanoparticles with excellent electrical and optical properties, Adv. Mater. 17 (2005) 1382–1386.
[32] T.-M. Wu, S.-H. Lin, Characterization and electrical properties of polypyrrole/multiwalled carbon nanotube composites synthesized by in situ chemical oxidative polymerization, J. Polym. Sci. B: Polym. Phys. 44 (2006) 1413–1418.
[33] M.R. Karim, C.J. Lee, A.M.S. Chowdhury, N. Nahar, M.S. Lee, Radiolytic synthesis of conducting polypyrrole/carbon nanotube composites, Mater. Lett. 61 (2007) 1688–1692.
[34] J. Liu, M. Wan, Composites of polypyrrole with conducting and ferromagnetic behaviours, J. Polym. Sci. A: Polym. Chem. 38 (2000) 2734–2739.
[35] K. Cheah, M. Forsyth, V.T. Truong, Ordering and stability in conducting polypyrrole, Synth. Met. 94 (2) (1998) 215–219.
[36] O.A. Kuznetsov, O.N. Sorokina, V.G. Leontiev, O.A. Shlyakhtin, A.L. Kovarski, A.A. Kuznetsov, ESR study of thermal demagnetization processes in ferromagnetic nanoparticles with curie temperatures between 40 and 60 °C, J. Magn. Magn. Mater. 311 (2007) 204–207.
[37] V.V. Srinivasu, S.E. Lofland, S.M. Bhagat, Room temperature colossal microwave magnetoimpedance in micron size powders of $La_{0.7}Ba_{0.3}MnO_3$ and $La_{0.7}Sr_{0.3}MnO_3$ – a novel magnetic tape, J. Appl. Phys. 83 (1998) 2866–2868.
[38] Y. Koseoglu, B. Aktas, ESR studies on superparamagnetic $Fe_3O_4$ nano particles, Phys. Status Solidi C 1 (2004) 3516–3520.
[39] S. Dey, S. Goswami, U.C. Ghosh, Hydrous ferric oxide (HFO) – a scavenger for fluoride from contaminated water, Water Air Soil Pollut. 158 (2004) 311–323.
[40] C.S. Sundaram, N. Viswanathan, S. Meenakshi, Uptake of fluoride by nano-hydroxyapatite/chitosan, a bioinorganic composite, Bioresour. Technol. 99 (2008) 8226–8230.
[41] Y.H. Li, S. Wang, X. Zang, J. Wei, C. Xu, Z. Luan, D. Wu, Adsorption of fluoride from water by aligned carbon nano tubes, Mater. Res. Bull. 38 (2003) 469–476.
[42] X. Zhao, J. Wang, F. Wu, T. Wang, Y. Cai, Y. Shi, G. Jiang, Removal of fluoride from aqueous media by $Fe_3O_4$@$Al(OH)_3$ magnetic nanoparticles, J. Hazard. Mater. 173 (2010) 102–109.
[43] I. Abe, S. Iwasaki, T. Tokimoto, N. Kawasaki, T. Nakamura, S. Tanada, Adsorption of fluoride ions onto carbonaceous materials, J. Colloid Interface Sci. 275 (2004) 35–39.
[44] K. Biswas, K. Gupta, U.C. Ghosh, Adsorption of fluoride by hydrous iron (III)–tin(IV) bimetal mixed oxide from the aqueous solutions, Chem. Eng. J. 149 (1–3) (2009) 196–206.
[45] A. Bansiwal, D. Thakre, N. Labhshetwar, S. Meshram, S. Rayalu, Fluoride removal using lanthanum incorporated chitosan beads, Colloids Surf. B: Biointerfaces 74 (2009) 216–224.
[46] Y.H. Li, S. Wang, A. Cao, D. Zhao, X. Zhang, C. Xu, Z. Luan, D. Ruan, J. Liang, D. Wu, B. Wei, Adsorption of fluoride from water by amorphous alumina supported on carbon nanotubes, Chem. Phys. Lett. 350 (2001) 412–416.
[47] W. Ma, F.Q. Ya, M. Han, R. Wang, Characteristics of equilibrium, kinetics studies for adsorption of fluoride on magnetic-chitosan particle, J. Hazard. Mater. 143 (2007) 296–302.
[48] A. Eskandarpour, M.S. Onyango, A. Ochieng, S. Asai, Removal of fluoride ions from aqueous solution at low pH using schwertmannite, J. Hazard. Mater. 152 (2008) 571–579.
[49] S. Kagne, S. Jagtap, P. Dhawade, S.P. Kamble, S. Devotta, S.S. Rayalu, Hydrated cement: a promising adsorbent for the removal of fluoride from aqueous solution, J. Hazard. Mater. 154 (2008) 88–95.